Thermodynamic Optimization of Proton Exchange Membrane Fuel Cell System

S. O. Obayopo, T. Bello-Ochende and J. P. Meyer

Department of Mechanical and Aeronautical Engineering, University of Pretoria, Pretoria 0002, South Africa

Centre for Renewable and Sustainable Energy Studies

Abstract:

The proton exchange membrane (PEM) fuel cell is a promising candidate as zero-emission alternative power source for transport and stationary applications due to its high efficiency, low-temperature operation, high power density, quick-start up and system robustness. However, before this class of energy becomes competitive with traditional fossil fuel powered combustion engines, its performance and cost must be optimized. This study shows a three dimensional optimization study for a PEM fuel cell under different operating conditions and channel geometries. The continuity, momentum, energy and species conservation equations describing the flow and species transport of the gas mixture in the coupled gas channels and the electrodes were numerically solved using a computational fluid dynamics code. The effect of various operating parameters and channel geometries on the performance of the fuel cell was analysed. Results were validated by comparing the predicted results with experimental results published in the literature and were found to be in good agreement. The result obtained would lead to improvements in the design of fuel cells.

Keywords: PEM fuel cells; optimization; parameters; geometry; performance

Introduction

Fossil fuel usage has caused great environmental concern in recent years, such as the greenhouse effect and climate change. The increasing pollution in the environment due to these fossil sources has necessitated the search for other more efficient and cleaner alternatives for power generation. Fuel cell has been identified as a viable alternative for power generation purposes due to its efficiency and cleanliness. The fuel cell technology is environmentally friendly, requires low maintenance for the component parts and high theoretical efficiency due to direct conversion of energy. Fuel cell is being developed for a wide range of applications depending on the size and operating temperature.

Proton exchange fuel cells (PEMFCs), using hydrogen is one emerging fuel cells with many advantages ranging from emission of water as waste, operation at low temperature for quick start-up, and uses solid polymer as electrolytes which reduces both construction and safety complications. This fuel cell type is highly being considered as an alternative power source for stationary and mobile applications. However, the large initial capital costs of fuel cell technology have offset the advantages it offers and slowed down its adoption for widespread applications (Rowe and Li, 2001; Siegel et al., 2003). Model development has paved ways for the development of this new energy system especially in the area of cost reduction. In addition, the expensive experimental procedures for studying the performance of fuel cells have greatly stimulated interest in efforts to develop models that could

Nomenclature

C_i	[kg kg^{-1}]	mass fraction of chemical species
C_p	[J kg^{-1} K^{-1}]	Constant-pressure heat capacity
D_i^{eff}	[m^2 s^{-1}]	effective diffusion coefficient of species *i*
E_{OCV}	[V]	open circuit voltage
F	[Cmol^{-1}]	Faraday constant (96,487 C mol^{-1})
Flwr	[kg/s]	flowrate
h_{react}	[J Kmol^{-1}]	Enthalpy of electrochemical reactions
h_L	[J kg^{-1}]	enthalpy of condensation/vaporization of water
I	[A m^{-2}]	exchange current density
i_o	[Am^{-2}]	local current density
n		electron number
p	[Pa]	pressure
Por		porosity
R	[mol^{-1} K^{-1}]	universal gas constant (8.314J mol^{-1} K^{-1})
R_{ohm}	[Ω m]	ohm resistivity
$R_{an,\ cat}$	[A m^{-3}]	volumetric transfer current at anode and cathode
S		source term
t	[s]	time
T	[K]	temperature
V	[V]	cell voltage
v	[m/s]	components of velocity
x, y, z	[m]	coordinate

Greek symbols

α_{an}		electrical transfer coefficient (anode)
α_{cat}		electrical transfer coefficient (cathode)
β	[m^2]	permeability
μ	[kg m^{-1} s^{-1}]	fluid viscosity
ε		porosity of porous media
η	[V]	overpotential
λ^{eff}		effective heat conductivity
μ^{eff}	[kg s m^{-2}]	Effective dynamic viscosity
Φ	[V]	phase potential function
ρ	[kg m^{-3}]	density

Subscripts and superscripts

an	anode
cat	cathode
e	electrolyte
e^-	electrochemical reaction of hydrogen
O_2	oxygen
H_2	hydrogen

H_2O	water
i	species
m	mass
ohm	ohmic
opt	optimum
ref	reference value
s	electronic conductive solid matrix
u	momentum
z	species value at reaction sites for 0,1,2,3 domains of the cell

effectively simulate and predict reactant transport, heat and mass transfer using computational fluid dynamics.

Fuel cell modeling has received tremendous attention in the last two decades with the ultimate aim of better understanding of the underlying phenomenon during the working operation of fuel cells. In the landmark works on PEMFC (Bernardi, 1990; Bernardi and Verbrugge, 1991 and Springer et al., 1991) which are based on one-dimensional models, the focus is on humidification requirements of inlet gases and issues related to variable membrane humidification. The work by the groups provided the required framework for the multidimensional models that followed in subsequent years. Subsequently, numerous studies have been carried out focusing on issues ranging from cell performance, water and thermal management in the fuel cell system. A vast number of the works are also CFD based (Ju et al., 2005; Yong et al., 1994; Marr and Li, 1998; Dutta et al., 2001; Yan et al., 2006; Lin et al., 2006; Zhang et al., 2008). Most fuel cell models in the literature focused on numerical simulation of transport phenomenon and parametric study of the effects of physical variables, thus these models attempt to present a range of values of operating conditions for examined models and only a few works ascertained optimal operating conditions for their model. Lin et al. (2006) worked on optimal channel width ratio, porosity of gas diffusion layer and catalyst layer porosity on fuel cell performance. The result presents an optimal design under specific operating condition for the investigated parameters. Similarly, Zhang et al (2008) also presents a three-dimensional mathematical model to investigate the optimal parameters for fuel cell performance considering porosity, permeability, thickness of the gas diffusion layer and the inlet gas stoichiometry using Powell algorithm. Results from their study provided an optimal search for a typical value of the fuel cell voltage.

Information on the analysis of fuel cells in three-dimensions which incorporates the determination of optimal operating values for a specific fuel cell design is still very limited in the literature. The purpose of this study is to investigate the effect of operating conditions such as temperature, pressure, porosity, reactant flow rates and channel geometry (width and depth) on a single PEM fuel cells performance and also to determine the optimal operating condition for this class of fuel cell. This will subsequently add to the knowledge base needed to produce generic design information for fuel cell systems, which can be applied to better designs of fuel cell stacks.

2. Model description

In the modeling of the fuel cell the following assumptions were made: the cell operates under steady-state condition, isothermal boundary conditions were used for external walls, flow in the cell is considered to be laminar, reactant and products are

assumed to be ideal gas mixtures, and the electrode is assumed to be an isotropic and homogenous porous medium. Figure 1 shows a schematic diagram of a typical PEM fuel cell consisting of nine different regions. It was assumed that the fuel was hydrogen at the anode side, diffuses through the porous gas diffusion layers and come in contact with the catalyst layer. At this layer, it forms hydrogen ions and electrons. The hydrogen ions diffuse through the polymer electrolyte membrane at the centre while the electrons flow through the gas diffusion layer to the current collectors and into the electric load attached. The electrochemical reactions are:

anodic: $$H_2 \rightarrow 2H^+ + 2e^- \quad (1)$$

cathodic: $$\frac{1}{2}O_2 + 2H^+ + 2e^- \rightarrow H_2O \quad (2)$$

net-reaction: $$H_2 + \frac{1}{2}O_2 \rightarrow H_2O \quad (3)$$

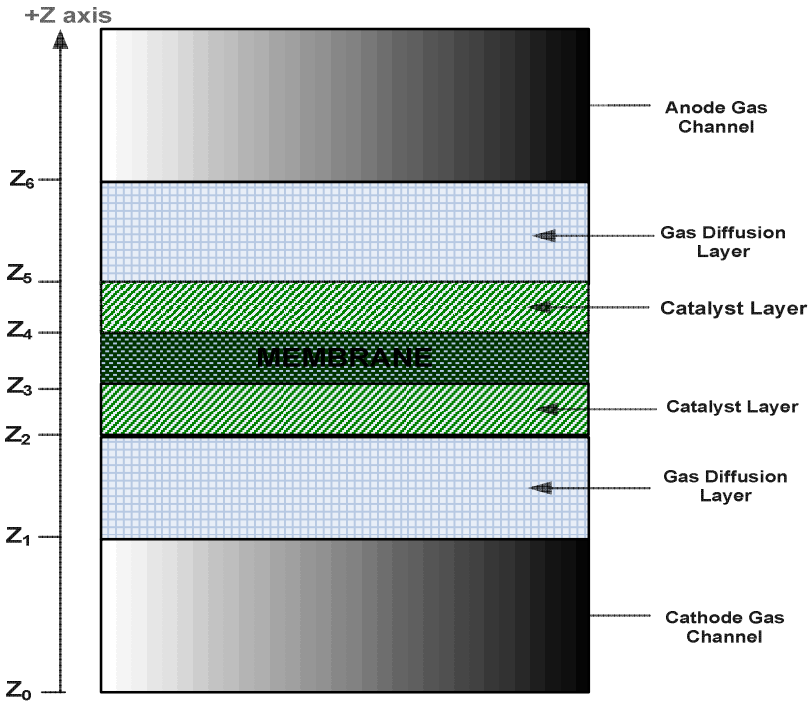

Figure 1 Schematic diagram of a single PEM fuel cell

Figure 2 depicts the computational domain consisting of the anode flow channel, anode diffusion layer, MEA assembly, cathode diffusion layer, and cathode flow channel. In this model, the numerical domain is a full single cell geometry domain. Fuel cell performance was evaluated at operating temperatures from 65 to 90^{o}C, operating pressure from 1 to 5 atm, electrode porosities from 0.3 to 0.7 and mass flow rates at the oxygen cathode from 5.0e^{-06} to 1.6.0e^{-04} kg/s. The channel width was varied from 0.6 to 1.6 mm resulting in 6 cases (0.6, 0.8, 1.0, 1.2, 1.4, 1.6) while the channel depth was varied from 0.5 to 3.0 mm (0.5, 1.0, 1.5, 2.0, 2.5, 3.0). The length of the channel was kept at 100 mm. Pure hydrogen and air was used as reactant gases in the model. A counter-flow inlet/outlet configuration was used in this study and the operating pressure was 101 kPa absolute at the exit of the cell. The details of the flow-field and other physical parameters used for the base case are summarized in Table 1.

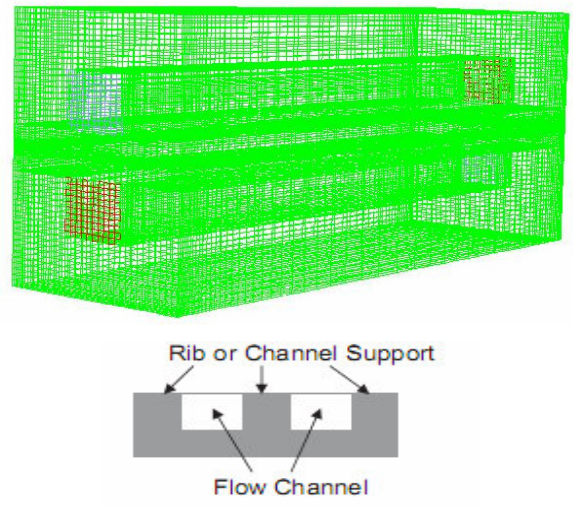

Figure 2 The discretized three dimensional computational domain of a single PEM fuel cell and flow-channel cross-section.

Table 1 Physical parameters and properties

Channel length (mm)	100
Channel width (mm)	1.0
Channel height (mm)	0.8
Membrane thickness (mm)	0.036
Catalyst layer thickness (mm)	0.012
Anode diffusion layer thickness (mm)	0.21
Cathode diffusion layer thickness (mm)	0.21
Membrane Porosity	0.4
Permeability (m^2)	1.76×10^{-11}
Oxygen mole fraction	0.406
Cell operating temperature (^oC)	70
Air-side/fuel-side inlet pressure (atm)	3/3
Open circuit voltage (V)	0.95
O_2 stochiometry ratio	1.2
H_2 stochiometry ratio	2.0
Relative humidity of inlet fuel/air	100%
Reference current density of anode (A/m^2)	7500
Reference current density of cathode (A/m^2)	20

Anode transfer coefficient	2.0
Cathode transfer coefficient	2.0

2.1 Model equations

The basic transport equation (conservation of mass and momentum) apply to the transport of gas mixtures in the gas channels in the fuel cell. The corresponding governing equations are as follows:

Continuum equation:

$$\frac{\partial(\varepsilon\rho)}{\partial t} + \nabla \cdot (\varepsilon\rho u) = S_m \tag{4}$$

Momentum equation:

$$\frac{\partial(\varepsilon\rho u)}{\partial t} + \nabla \cdot (\varepsilon\rho uu) = -\varepsilon\nabla p + \nabla \cdot (\varepsilon\mu^{eff}\nabla u) + S_u \tag{5}$$

Species conservation equation:

$$\frac{\partial(\varepsilon\rho c_i)}{\partial t} + \nabla \cdot (\varepsilon\rho u c_i) = \nabla \cdot (-\rho D_i^{eff}\nabla c_i) + S_i \tag{6}$$

Energy conservation equation:

$$\frac{\partial(\rho C_p T)}{\partial t} + \nabla \cdot (\rho u C_p T) = \nabla \cdot (\lambda^{eff}\nabla T) + S_T \tag{7}$$

The energy source term, S_T depicts the sum of the reversible heat release and the irreversible heat generation (Ju et al., 2005). In the catalyst layer, the reversible and irreversible reaction heats as well as latent heat of water phase change are considered; for the membrane, ohm heating of current due to large resistance of the membrane is also considered. The total source that is accounted for in the thermal energy equation is:

$$S_T = h_{react} - R_{an,cat}\eta_{an,cat} + I^2 R_{ohm} + h_L \tag{8}$$

where h_{react} is net enthalpy change due to the electrochemical reactions,

$R_{an,cat}\eta_{an,cat}$ is the product of the transfer current and the overpotential in the anode or the cathode catalyst layer,

R_{ohm} is the ohmic resistivity of the conducting media, and

h_L *is* the enthalpy change due to condensation/vaporization of water.

The source terms account for situations when a fluid passes through a porous medium. In this paper, the term is applicable to the electrode and catalyst zones. For low velocities encountered in fuel cells, these source terms which are applicable at the gas diffusion layers and are given by Darcy's law:

$$S_{px} = -\frac{\mu v_x}{\beta_x}; \quad (9)$$

$$S_{py} = -\frac{\mu v_y}{\beta_y}; \quad (10)$$

$$S_{pz} = -\frac{\mu v_z}{\beta_z}; \quad (11)$$

at $z_1 \leq z \leq z_6$

where μ is the fluid viscosity in the medium and β is the permeability of the electrode material. The permeability of the medium was assumed to be isotropic as stated in the assumptions in this model hence; β_x, β_y and β_z all have the same value stated in table 1 (1.76 x 10^{-11} m^2). Other source terms for these equations above used in the model were taken from Dutta et al. (2001). The local current density i_o is a measure of the electrochemical reaction rate and generally given by the Butler-Volmer equation:

$$i_o = i_{o,ref}\left\{\exp\left[\frac{\alpha_{an} nF}{RT}\eta\right] - \exp\left[\frac{-\alpha_{cat} nF}{RT}\eta\right]\right\} \quad (12)$$

where η is the overpotential and defined as,

$$\eta = \left(\Phi_s - \Phi_e\right) - E_{ocv} \quad (13)$$

F is the Faraday constant, α_{an} and α_{cat} represents the experimental anodic and cathodic transfer coefficient, respectively; and R is the universal gas constant.

2.2 Boundary conditions

Pressure boundary conditions were specified at the outlets since the reactant gas flow is usually separate and at different pressures. The inlets were all assigned as mass flow inlets. The gas diffusion layer and the catalyst layer were surrounded by sealed plates at the inlet and outlet plane, so the boundary conditions at the inlet and outlet planes take the no-slip condition for the velocity and non-permeable condition for the species mass fraction. The membrane-electrode interface was defined as a wall, primarily to inhibit species and electron crossover through the membrane. These also prevent pressure problems at this interface. In the areas at which the gas diffusion electrodes were in contact with the bipolar plates, a constant reference voltage equal to zero was assigned as a boundary condition both at the anode and at the cathode. The electron flux was set to zero at all other walls. The anode was grounded (V = 0) and the cathode terminal was set at a fixed potential (0.75 V) less than the open-circuit potential (0.95 V). Both anode and cathode terminals were assigned wall boundaries.

2.3 Solution technique

The model equations were solved using the commercial computational fluid dynamics (CFD) software ANSYS Fluent® 12.0 with Gambit® (2.4.6) as a pre-processor. The CFD code has an add-on package for fuel cells, which has the requirement of the source terms for species transport equations, heat sources, and liquid water formation (Ansys 2009). Control volume technique was used for solving

the problem. The meshes were more refined at the membrane/catalyst assembly regions. The conservation of mass, momentum and energy equations in the three-dimensions were solved, in turn, until the iterative process meets the convergence criteria. In this study, the definition of convergence criteria indicates that the largest relative error between consecutively two iterative residuals within the overall computational domains is less that 10^{-6}. The domain was divided into hexahedral volume elements. A computational mesh of about 130 000 volume elements was obtained as the grid. A grid adaptation technique was employed to insure that solutions were independent of the dimensions of the chosen grid with consideration for both accuracy and economics. The number of the grid cells was decreased and increased by 50% of the base case and the predicted results varied by less than 2%, which indicated that the results presented was grid independent. The solution strategy was based on the SIMPLE algorithm (Pantakar, 1980). Momentum equations were solved for the velocity followed by solving the equation of continuity, which updates the pressure and the flow rate. Results were then verified for convergence. The simulation for each operating potential converged in 25 - 30 minutes on an Intel® Core(TM) 2Duo 3.00 GHz with 3.24 GB of DDRam.

3. Results and discussion

3.1 Code validation

The base case was used to perform a series of simulations from a low operating current density to a high operating current density to validate the model used in this paper. The polarization curve shown in Figure 3 shows strong agreement between predicted results and the experimental data published in the literature (Wang et al., 2003). The predicted curve agrees well with experimental measurement at low current densities but at high current density there is some level of variation between the results. The maximum percentage difference between the numerical and the experimental was below 2.2%. This might be due to various factors ranging from the assumption that there is no liquid water formation at the electrode sites to not making provision for contact electrical resistances within components in the numerical model. The disparity shows that the present model overestimates the fuel cell performance due to neglect of the liquid water formation at the cathode. Nonetheless, the prediction from the model could still successfully be used for better understanding of the complicated processes in fuel cell system.

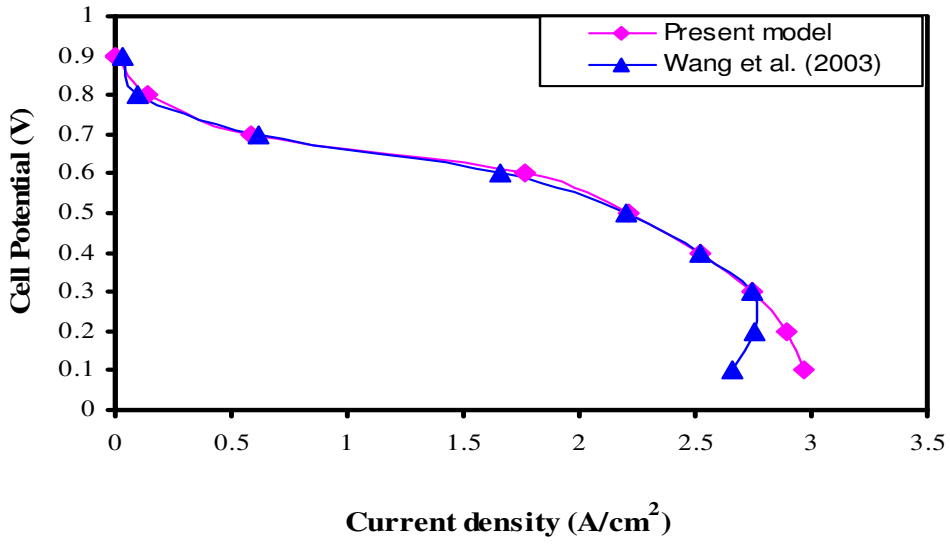

Figure 3 Comparison of numerical model and experimental polarization curves.

3.2 Effects of operating temperature

Figure 4 illustrates the obtained polarization curves obtained from the model at several operating temperatures from 65 to 90 °C at stochiometry ratios of 1.2 and 2.0 respectively for the anode and the cathode**.** The curve indicates that the fuel cell performance is an optimum at temperatures at approximately 65 to 75 °C. This is consistent with literature (Marr and Li, 1998; Yan et al., 2006). This increase in the fuel cell performance is attributable to an increase in gas diffusivity and membrane conductivity at higher operating temperatures.

The polarization curves are also lower at 75 - 80 °C compared to 65 - 75 °C in the lower current density region, primarily due to the lower reaction rates resulting in low water content in the membrane. The condensation of water easily occurs at lower temperatures resulting to flooding and deteriorates gas diffusivity in the catalyst layer and the gas diffusion layers. As shown also on the curve at temperatures beyond 80 °C, is that the cell performance declines, because membrane conductivity decreases at high temperatures due to the onset of reduction in relative humidity of reactant gases and water content in the membrane. Hence, the fuel cell performance is adversely affected at temperatures between 85 and 90 °C.

Increasing the cell temperature beyond 85 °C could result in higher levels of water loss in the cell until a critical temperature is attained where the evaporated water is greater than the amount being generated in the cell thereby resulting in total dry-out of the membrane. This could eventually lead to fuel cell failure. This model ascertains the facts that these fuel cells need be operated at temperatures below 80 °C. A humidifier may be required if operation at higher temperature is required but this adds to the capital and running costs of fuel cells.

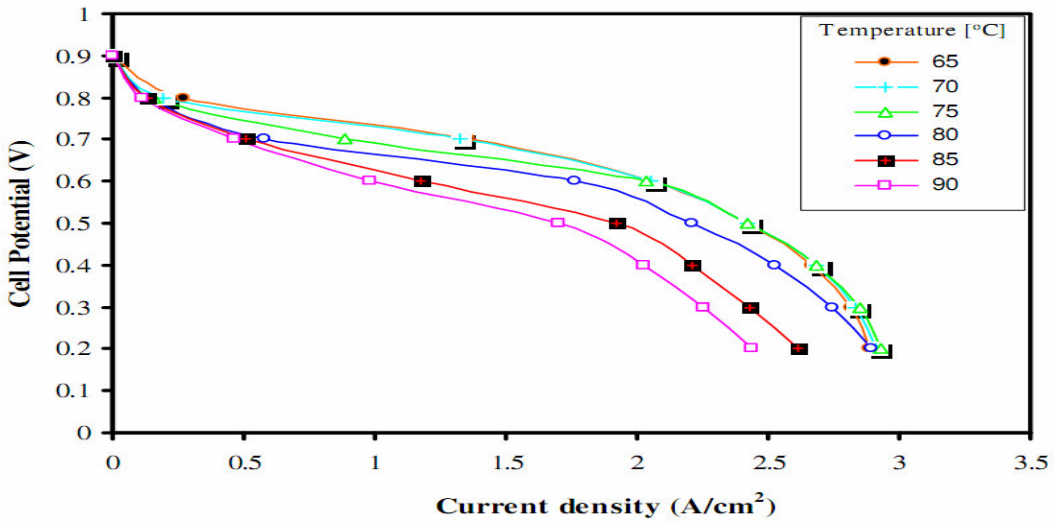

Figure 4 Effect of temperature on cell performance at base conditions.

3.3 Effect of operating pressure

Fuel cell performance is also largely influenced by operating pressure. In this study, operating pressure was varied from 1 to 5 atm at a constant operating temperature of 70 °C. The polarisation curves for different operating pressure are shown in Figure 5. As operating pressure was increased from 1 to 5 atm, the fuel cell performance also improved. There was a significant increase in the fuel cell performance from 1 atm to 3 atm; however after 3 atm the increase was minimal. Increasing pressure improves the reactants interaction with the electrolyte hence increasing fuel cell performance.

Pressure impact on the fuel cell performance is prominent at higher current density of operation. Generally the polarization curve shift position positively as the pressure increase.

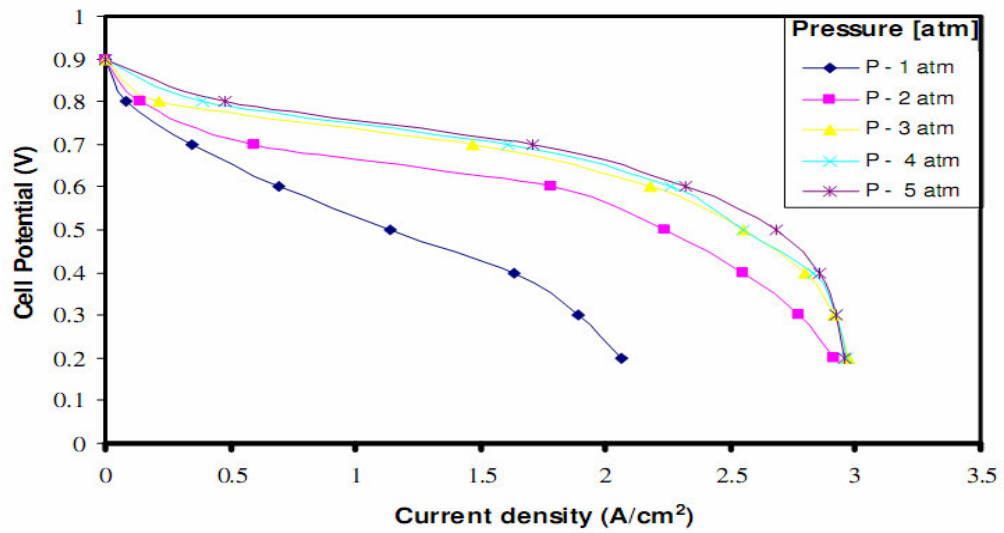

Figure 5 Effect of operating pressure on cell performance at base conditions.

3.4 Effect of gas distribution electrode porosity

Porosity of electrodes is another sensitive parameter affecting fuel cell performance. A larger porosity gives room for more space for gas diffusion, which could also lead to high contact resistances in the fuel cell. Hence, for best performance of fuel cell there must be an optimal porosity level for the gas electrodes. Figure 6 displays the changes in the fuel cell performance with different values of gas electrode porosities at a constant operating temperature of 70 ^{o}C and pressure of 3 atm. Reduction in porosities of the gas distribution electrodes results in a decrease in fuel cell performance. Though not quite discernable in the figure, reducing porosity from 0.6 to 0.4 resulted in a 3.3 % decrease in the average current density for a fuel cell operated at 0.75 V.

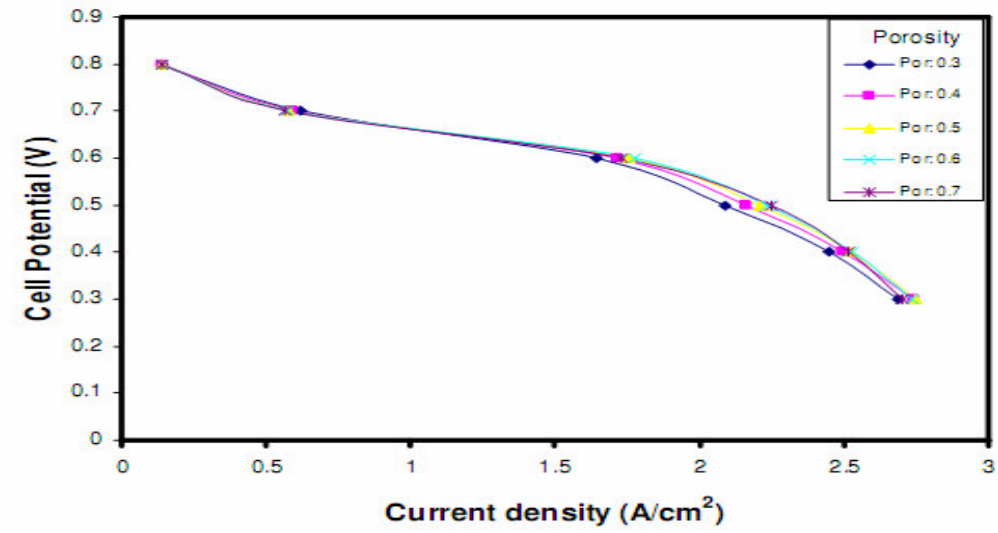

Figure 6 Effect of gas electrode porosity on cell performance at base conditions.

Though also quite minimal, porosity effect on fuel cell performance is more significant at lower porosities (0.3 to 0.4) for cells operating at higher current density. At higher porosity values (0.6 to 0.7), the effect on performance is quite negligible for fuel cells being operated at the same high current densities. This could be as a result of an increase in contact electrical resistance at the reaction sites despite the increase in the species transport due to larger diffusion pores. The use of high electrode porosity in practice might be limited by the need for structural integrity considerations of electrodes under required high pressure for fuel cell sealing.

3.5 Effect of cathode gas flow rate

Figure 7 shows the effect of changing the oxygen flow rate on the fuel cell performance. It is observed that when the cathode flow gas is increased, the fuel cell performance is enhanced especially at lower operating fuel cell voltages. The reason is due to the fact that there is an increase in oxygen gas through the gas diffusion layer to the reaction sites, which increases the rate of reaction.

At low operating voltages more liquid water is produced due to stronger electrochemical reaction rates, which is expected to reduce fuel cell performance. However, the high oxygen mass flow rates in the porous layer generate high shear forces, which aid the transport of liquid water downstream at the flow channel along the flow direction. The effect is minimal at high operating voltages as observed on the curves primarily due to low membrane humidification since low amounts of water presence occur at this voltage levels due to slow reaction rates resulting in reduced cell performance.

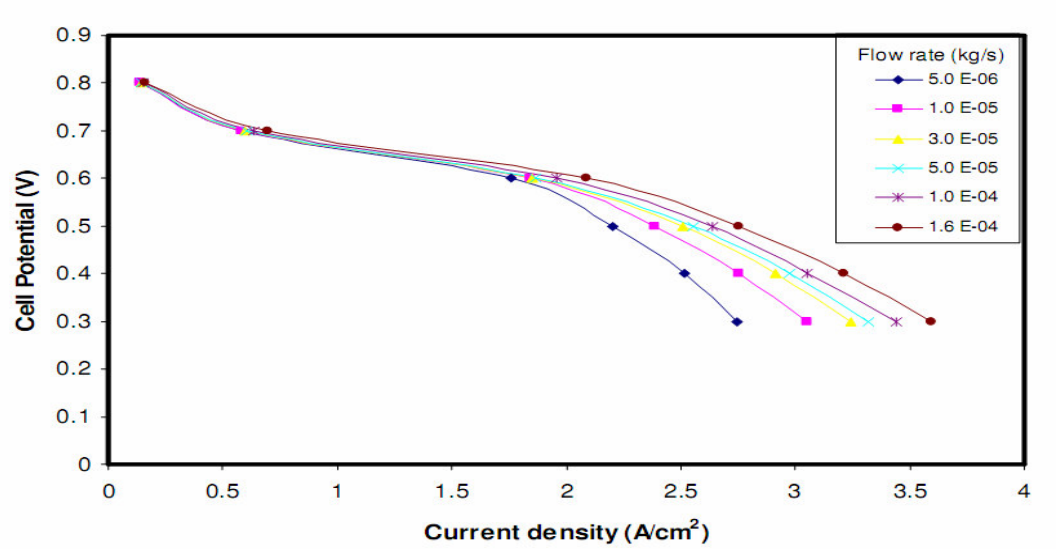

Figure 7 Effect of cathode gas flow rate on cell performance at base conditions.

3.6 Effect of channel width and depth

Figure 8a illustrates the effect of channel depth on the fuel cell performance at constant channel length. The optimal current density for the fuel cell was obtained at channel depth of 2.0 mm (current density: 2.62 A/cm^2). Further increase in depth shows a decline in fuel cell performance. Figure 8b shows the fuel cell performance for the 6 cases of channel width considered. Performance increases gradually from case 1 (0.6mm – current density: 1.30 A/cm^2) until an optimum is reached at case 4 (1.2mm – current density: 2.45 A/cm^2). Increasing the channel width beyond 1.2 mm shows a reduction in fuel cell performance. These results were consistent with those observed by other researchers in their work. Watkins et al (1991) studied optimal

dimension for cathode side channel of the fuel cell. They claimed the most preferred ranges to be 1.02- 2.04 mm for channel depth and 1.14-1.4 mm for channel width.

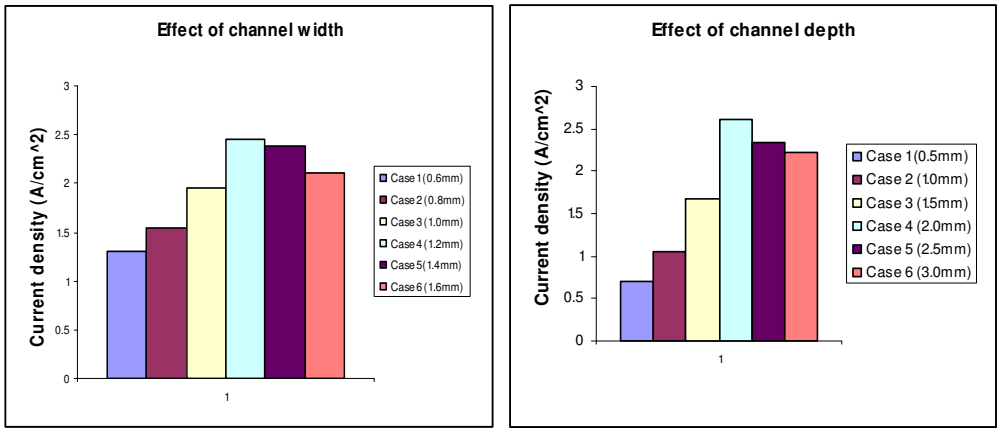

Figure 8 (a) Effect of channel depth on cell performance at base case condition and (b) Effect of channel width on cell performance at base case condition.

4. Optimal operating parameters

In this section, we determined the optimal operating conditions for the developed model. The simulation work in the previous sections (3.2 - 3.5) suggested the presence of an optimal for operating the fuel cell. The sets of the initial ranges of values for the parameters examined were re-evaluated through a series of numerical optimisation and calculations to determine an optimum value for the model under consideration in Figure 1. Results are presented in order to show how each parameter behaves at 0.3 V of operating cell voltage (OCV). This will assist in determining the best values of the operating parameters for the fuel cell system at the chosen levels of the operating voltage.

Figure 9 to Figure 12 depicts the optimal search graphs for all the five parameters examined for this model. Figure 9 shows the optimal current density obtained at temperatures of 75 ^{o}C at 0.3 operating cell voltage. In Figure 10, optimal current density was obtained at pressure level of 3.23 atm. The figure also shows that

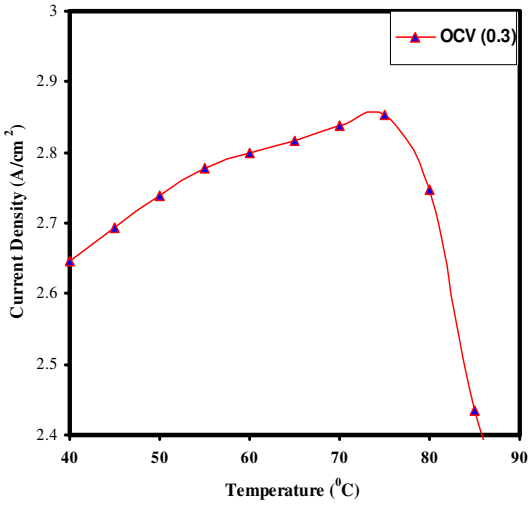

Figure 9 The cell current density as a function of temperature and the operating cell voltage.

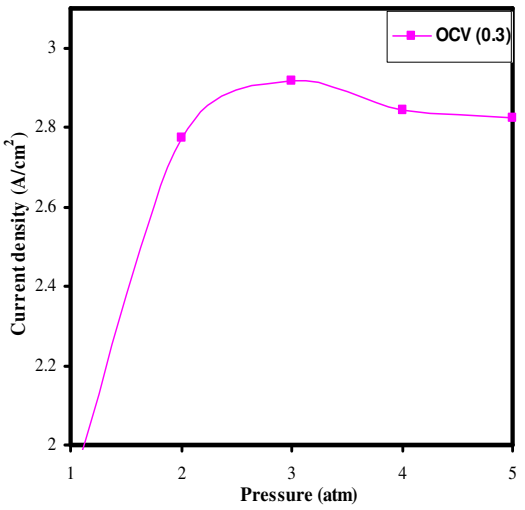

Figure 10 The cell current density as a function of pressure and the operating cell voltage.

increase in pressures beyond certain levels at these operating voltages shows no significant effect on performance. Figure 11 shows optimal for the porosities. At 0.3 operating cell voltage, optimal was obtained at 0.62 porosity level. There was no distinct optimal for cathode flow rates as shown in Figure 12. Optimal performance for the fuel cell lies at 1.55E-04 (kg/s) cathode flow rate. Table 2 summarises the values of the optimal operating parameters from the numerous simulations at 0.3 V of operation.

In Figure 13 (a-d), the contours of hydrogen mass fractions were depicted at these optimal operating values for 0.3 V operating fuel cell voltages. In the contours, the flow in the anode channel containing hydrogen gas is from left to right and the mass fraction of hydrogen decreases in the direction of flow primarily due to water being pulled through the membrane along with hydrogen as it is being utilized in the fuel cell.

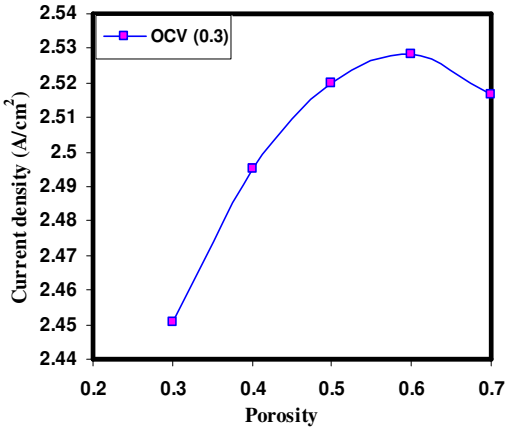

Figure 11 The cell current density as a function of electrode porosity and the operating cell voltage.

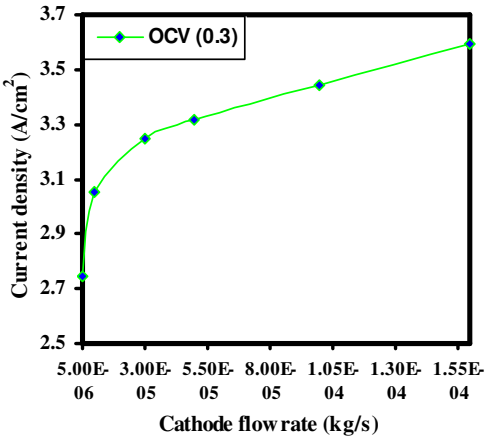

Figure 12 The cell current density as a function of cathode gas flow rate and the operating cell voltage.

Table 2 Optimal parameter values for the model

Optimal Parameters		Cell voltage (V) 0.3
Temperature (^{o}C),	T_{opt}	75
Pressure (atm),	P_{opt}	3.23
Porosity,	Por_{opt}	0.62
Cathode flow rate (kg/s), flwropt		1.60E-04

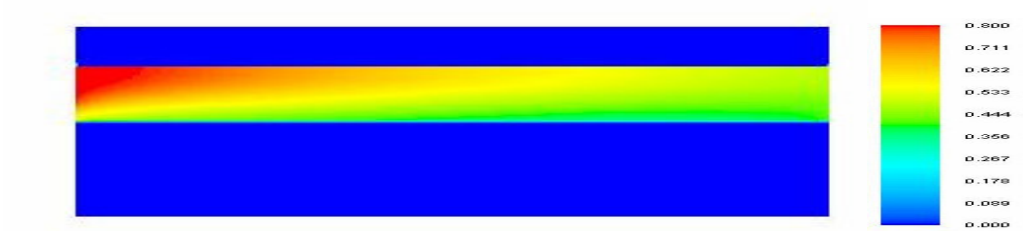

Figure 13 (a) Specie mass fraction of hydrogen at anode channel for T_{opt} = 75 ^{o}C.

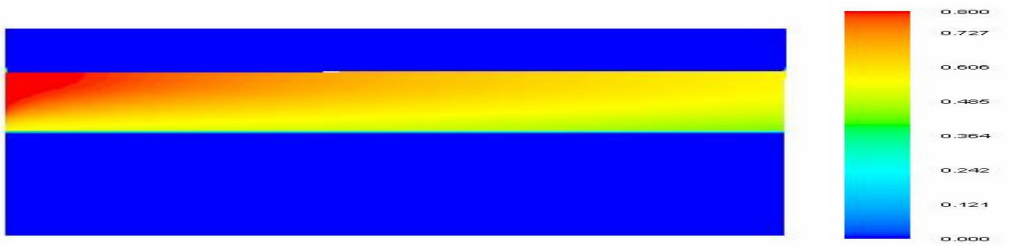

Figure 13 (b) Specie mass fraction of hydrogen at anode channel for P_{opt} = 3.23 atm.

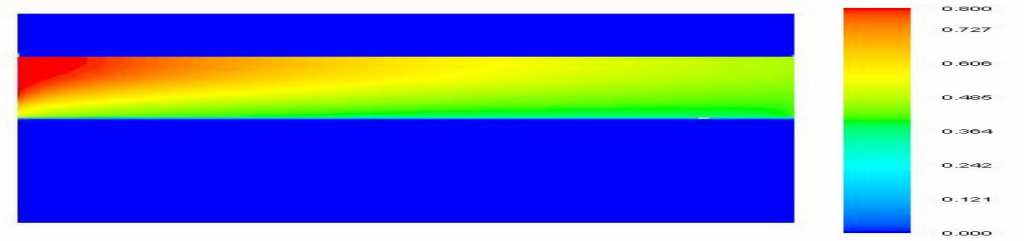

Figure 13 (c) Specie mass fraction of hydrogen at anode channel for Por_{opt} = 0.62

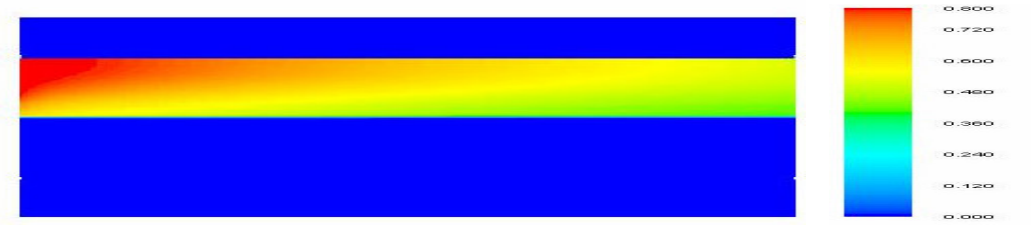

Figure 13 (d) Specie mass fraction of hydrogen at anode channel for **$flwt_{opt}$ = 1.60E-04**

5. Conclusion

In this paper, a steady-state three-dimensional computational model was established to study the performance of a single channel proton exchange fuel cell under varying operating conditions. The model prediction is validated by comparison with experimental data and was in good agreement. The numerical results provided detailed information on the effect of varying operating parameters of a single channel fuel cell performance. It was found that increasing the operating temperature enhances fuel cell performance though an optimal temperature exists after which performance is hindered due to membrane dry-out. The effect of operating pressure, electrode porosity, cathode flow rates, and feed gas stoichiometry also influence the fuel cell performance and were also investigated. The electrode porosity effect is more dominant at low operating cell voltages than at higher operating fuel cell voltages. The study also provides optimal operating values for the operating parameters in a single channel PEM fuel cell.

References

Ansys Fluent® 12.0. (2009). Users Guide Documentation, Ansys Inc., Southpointe, SAS.

Bernardi, D. M. (1990). Water balance calculations for solid polymer electrolyte fuel cells. *J. Electrochem.Soc.* 137 (11): 3344-3345.

Bernardi, D. M., & Verbrugge, M. W. (1991). Mathematical model of a gas diffusion electrode bonded to a polymer electrolyte. *AIChE J.* 37 (8): 1151-1163.

Dutta, S., Shimpalee, S., & Van Zee, J. W. (2001). Numerical prediction of mass exchange between cathode and anode channels in a PEM fuel cell. *Int. J. Heat Mass Transfer* 44: 2029-2042.

Ju, H., Meng, H., & Wang, C.Y. (2005). A single-phase, non-isothermal model for PEM fuel cells. *Int. J. Heat Mass Transfer* 48:1303-1315.

Lin, H. H., Cheng, C., Soong, C., Chen, F., Yan, W. (2006). Optimization of key parameters in the proton exchange membrane fuel cell. *J. Power Sources* 162: 246-254.

Marr, C., & Li, X. (1998). An engineering model of proton exchange membrane fuel cell performance. *ARI* 50:190-200.

Pantakar, S. V. (1980). *Numerical Heat Transfer and Fluid Flow.* New York: Hemisphere Publishing Corp.

Rowe, A., & Li, X. (2001). Mathematical modeling of proton exchange membrane fuel Cells. *J. Power Sources,* 102: 82-96.

Siegel, N.P., Ellis, M.W., Nelson, D. J., & von Spakovsky, M. R. (2003). Single domain PEMFC model based on agglomerate catalyst geometry. *J. Power Sources* 115: 81-89.

Springer, T. E., Zawodzinski, T. A., & Gottesfeld, S. (1991). Polymer electrolyte fuel cell model. *J. Electrochem. Soc.* 138 (8): 2334-2342.

Wang, L., Husar, A., Zhou, T., & Liu, H. (2003). A parametric Study of PEM fuel cell performance. *Int. J. Hydrogen Energy* 28: 1263-1272.

Watkins, D. S., Dircks, K. W., & Epp, D.G. (1991). Novel fuel cell fluid flow field plate, US Patent 4988583.

Yan, Q., Toghiani, H., & Causey, H. (2006). Steady state and dynamic performance of proton exchange membrane fuel cells (PEMFCs) under various operating conditions and load changes. *J. Power Sources* 161: 492-502.

Yong, W. R., Velev, O. A., & Srinivasan, S. (1994). Mass transport phenomena in proton exchange membrane fuel cells using O_2/He, O_2/Ar, and O_2/N_2 mixtures. *J. Electrochem. Soc.* 141 (8):2084-2096.

Zhang, Z., Wang, X., Zhang, X., & Jia, L. (2008). Optimizing the performance of a single PEM fuel cell. *J. Fuel Cell Science and Technology*. Vol. 5/ 031007-1.